Materials Research. 2026; 29: e20250636
DOI: https://doi.org/10.1590/1980-5373-MR-2025-0636

Functional Polypropylene Filaments for 3D Printing with Antiviral Properties Using a Glassy Ceramic ZnO–Al–Si–Na Additive

***Bruna Zappelino Camillo*[a]*, *Anderson de Carvalho Fernandes*[a], *Giovani Silveira de Magalhães Martins*[a], *Bibiana Matte*[b], *Anael Preman Krelling*[c], *Raíssa Santos*[d], *Sabrina Cremonini*[a], *Simone Rohr*[a], *Creciana Maria Endres*[a]**

[a]*Centro Universitário SENAI Santa Catarina (UniSENAI), Joinville, SC, Brasil.*
[b]*Núcleo Vitro, Porto Alegre, RS, Brasil.*
[c]*Instituto Federal de Santa Catarina, Joinville, SC, Brasil.*
[d]*Universidade Federal de Ciências da Saúde de Porto Alegre, Porto Alegre, RS, Brasil.*

Received: September 10, 2025; Revised: December 26, 2025; Accepted: March 07, 2026

Additive manufacturing (AM) is a powerful platform for developing functional materials with broad applications across healthcare, consumer goods and industrial sectors. This study presents a pioneering polypropylene (PP) filament enhanced with a ZnO-based glassy ceramic additive (Si–Na–Al matrix), specifically designed for 3D printing. Beyond introducing antiviral functionality, the formulation overcomes a long-standing limitation in AM of polyolefins, significantly improving printability by reducing thermal shrinkage and enhancing interlayer adhesion. PP composites were fabricated with 2%, 6%, and 10% additive loadings and evaluated for morphological (SEM-BSE), chemical (FTIR, EDS) and biological performance. Antiviral assays, conducted according to ISO 21702 using exposure times of 15 and 120 minutes, demonstrated viral load reductions of up to 99.68% against betacoronavirus (MHV-3) and 96.84% against adenovirus at the highest additive concentration. In contrast, antibacterial tests based on ISO 22196 against E. coli and S. aureus showed no significant activity, likely due to limited additive release from the polymer matrix. These results establish a novel antiviral 3D-printable PP composite with improved manufacturing performance, offering a versatile solution for applications demanding structural integrity combined with bioactive antiviral surfaces.

Keywords: *Additive Manufacturing, Polypropylene, Viral Inhibition, 3D Printing.*

1. Introduction

Additive Manufacturing (AM), also known as 3D printing, has emerged as a transformative technology across various industries, offering unprecedented design freedom and customization. In the healthcare sector, AM has gained substantial attention due to its potential to produce personalized biomedical devices, prosthetics, and implants, often incorporating antimicrobial and antiviral functionalities. In 2016, medical and dental applications represented approximately 12% of the AM market share by industry, and the sector is expected to surpass $3 billion by 2026[1,2].

Polypropylene (PP) is a thermoplastic polymer that has proven highly suitable for additive manufacturing in packaging and medical applications, due to its chemical resistance, mechanical strength, recyclability, and ability to preserve organoleptic and nutritional properties in food products[3,4]. Additionally, the development of bio-based PP and other bioplastics is expanding, aligning with the increasing demand for sustainable materials in global production[5].

Despite these advantages, printing polyolefins such as polypropylene via AM remains a significant challenge. Issues related to thermal compatibility, limited interlayer adhesion, and poor additive dispersion hinder the integration of antimicrobial functionality into PP-based 3D-printable formulations. Moreover, this work contributes to solving a long-standing challenge in 3D printing of polyolefins by enhancing the printability of polypropylene through ceramic-based additive modification.

Recent efforts have focused on incorporating antimicrobial agents, such as silver, copper, and zinc[6], as well as metal oxides[7], into polymer matrices to inhibit microbial growth[8-10]. However, traditional approaches often face limitations such as high cost, cytotoxicity, and difficulties in ensuring uniform dispersion or controlled release of active species[11,12]. To overcome these limitations, bionanocomposites have emerged as a promising class of materials. By combining biopolymers such as chitosan[13,14], starch, and carboxymethylcellulose[8] with nanostructured additives, it is possible to improve mechanical, thermal, and barrier properties while introducing effective antimicrobial activity.

Additionally, plant-derived polyphenolic compounds (e.g., gallic acid, caffeic acid, and tannic acid) have been employed to prevent bacterial adhesion in 3D-printed PET[15]. However, achieving an optimal balance between printability, stability, and antimicrobial functionality remains a critical bottleneck, especially for extrusion-based AM processes involving semi-crystalline polymers like PP.

*e-mail: zappelino.bruna@gmail.com
Associate Editor: Rodrigo Orefice.
Editor-in-Chief: Luiz Antonio Pessan.

In this context, this study introduces an innovative inorganic antimicrobial additive and evaluates its incorporation into polypropylene matrices for filament-based AM. The proposed approach, based on ceramic surface-functionalized particles, aims to enable antimicrobial functionality in PP while preserving printability, thereby broadening its potential applications in advanced packaging and biomedical domains.

2. Material and Methods

The PP used is a commercial heterophasic copolymer (impact copolymer) supplied by Braskem, grade H241, widely applied in extrusion and injection molding due to its enhanced impact resistance and processability. This PP was blended with a commercial additive formulated in a polyethylene (PE) masterbatch containing a ZnO-based glassy ceramic (Si–Na–Al matrix) supplied by Cristal Master. The material was processed using a gravimetric dosing and extrusion system. Before extrusion, PP and the ceramic-based masterbatch were dried at 80 °C for 4 h to remove moisture. The extrusion profile included multiple heating zones ranging from 160 °C to 250 °C, with typical values of 230–250 °C in the initial zones, gradually reduced to 170–200 °C in the latter zones, and 230–250 °C at the die (Gala matrix). The melt temperature was maintained at 215 °C, with a melt pressure of 35 bar and torque of approximately 150 A. A screw speed of 500 rpm was applied, using a screen pack configuration of 40/60/20 mesh. The degassing system included one open atmospheric vent and one closed vacuum vent, while water cooling was performed at 30 °C. The die configuration had 14 out of 19 holes open, producing filaments with a controlled diameter of 1.75 mm. The extrusion throughput was approximately 350 kg/h, ensuring uniform production of spools (~500 g each) later used for 3D printing of standardized test specimens. The mixture was extruded into filaments and used for 3D printing test specimens (Figure 1a). Four compositions were produced: pure PP and PP with 2%, 6%, and 10% additive. Before extrusion, PP and masterbatch were dried at 80 °C for 4 hours to remove moisture. Subsequently, filament coils (~500 g each) with a uniform diameter of 1.75 mm were fabricated for each composition, as exemplified in Figure 1 (b). Twenty standardized specimens (2 × 50 × 50 mm) per composition were then 3D-printed from these filaments, as illustrated in Figure 1b. Table 1 presents the parameters adopted for the fabrication of the specimens using the FDM process. Different nozzle temperatures were employed, one for each condition, to account for variations in material flow behavior and to optimize the print quality of each composition, particularly due to the addition of the additive. In addition to the nozzle temperature, several other printing parameters were carefully selected to ensure optimal fabrication quality. The bed temperature was adjusted to improve adhesion of the first layer and minimize warping, especially for semicrystalline polymers like polypropylene. The printing speed was set considering both material flow and dimensional accuracy, balancing faster production with the risk of defects. The cooling fan was used selectively to control the solidification rate of the extruded filament, influencing layer bonding and surface finish.

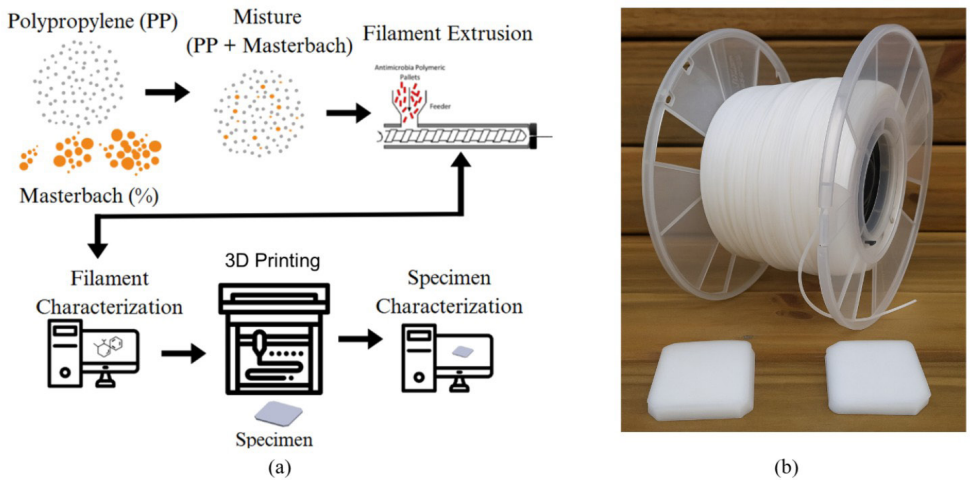

Figure 1. (a) Schematic of polypropylene composite fabrication with antimicrobial additives; (b) Extruded filament spool (~500 g, 1.75 mm diameter) of polypropylene containing 10% ZnO-based glassy ceramic additive (Si–Na–Al matrix), and corresponding 3D-printed test specimens (2 × 50 × 50 mm).

Table 1. Optimized FDM processing parameters used for neat PP and PP blends with additive.

Composition	Nozzle (°C)	Bed (°C)	Speed (mm/s)	Cooling Fan (%)	Layer Height (mm)	Retraction (Bowden)	Brim (mm)
Pure PP	240	90	40	0	0.3	4 mm	10
PP + 2%	242	90	40	0	0.3	4 mm	10
PP + 6%	244	90	40	5	0.3	4 mm	10
PP + 10%	247	90	40	5	0.3	4 mm	10

Layer height was chosen to provide a compromise between surface resolution and printing time, with finer layers promoting smoother surfaces and better feature definition. Retraction settings were optimized to reduce stringing and oozing, particularly in complex geometries. Finally, a brim was applied when necessary to further enhance bed adhesion and prevent edge lifting during the printing process. The values presented in Table 1 correspond to the parameters optimized to enable the printability of the specimens.

The same printed specimens were used for morphological (SEM, EDS) and chemical (FTIR) characterization, as well as for antimicrobial and antiviral assays, ensuring that all analyses were performed on identical surfaces and compositions. Particle size analysis of the inorganic additive was performed by SEM imaging using ImageJ software. Due to irregular particle morphology, the maximum linear dimension (Ferret's diameter) was measured for at least 50 randomly selected particles per sample condition (pure additive, and composites containing 2%, 6%, and 10% additive). Statistical comparisons among groups were conducted by one-way ANOVA at a 95% confidence level.

Post-processing characterization included Scanning Electron Microscopy with a Field Emission Gun (SEM-FEG), Energy Dispersive Spectroscopy (EDS), and Fourier-transform infrared spectroscopy (FTIR) using ATR mode to assess morphology and chemical composition.

Antimicrobial efficacy was evaluated per ISO 22196[16] focusing on *E. coli* and *S. aureus* (Figure 2). Sterilized samples were inoculated, covered with sterile films and incubated at 35 °C for 24 h under high humidity. Bacterial reduction was measured by colony counting, with antimicrobial performance expressed as inhibition percentage.

Antiviral evaluation followed ISO 21702[17] using two viral models: betacoronavirus (MHV-3), related to SARS-CoV-2, and adenovirus, a non-enveloped virus. Both were tested at 10^5 viral particles according to $TCID_{50}$ method. VERO and L929 cells were cultured in Dulbecco's Modified Eagle's Medium (DMEM) at 37°C with 5% CO_2 under laminar flow. Samples were exposed for 15 and 120 min, followed by viral activity quantification. Cytotoxicity was assessed after 24 h by cell imaging. Viral titration, based on cytopathogenic effects, quantified viral multiplication. Antiviral activity (R) was calculated as the log difference between control (U_t) and treated (A_t) samples.

$$R = U_t - A_t \quad (1)$$

3. Results and Discussions

Polypropylene (PP), like other polyolefins, typically exhibits high thermal shrinkage during 3D printing, resulting in warping, poor layer adhesion and dimensional instability.

This behavior is evident in Figure 3a, where the pure PP sample shows significant deformation after printing. The addition of 2% of the ceramic-based additive, composed of ZnO-based glassy ceramic additive, significantly improved the printability of PP, as shown in Figure 3b.

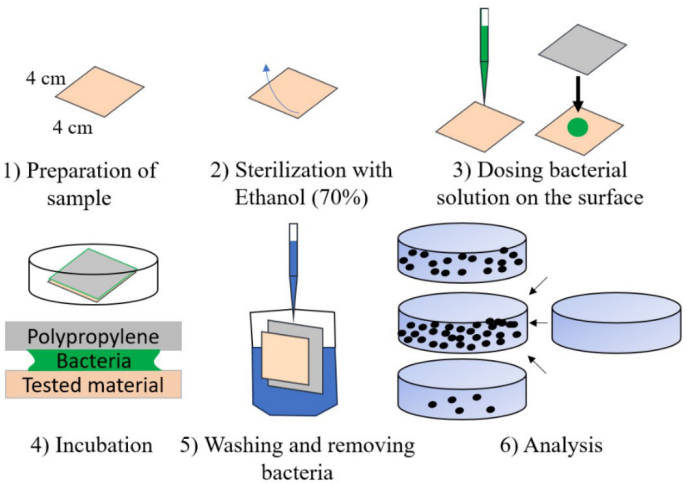

Figure 2. Inoculation procedure for antimicrobial and antiviral assessments.

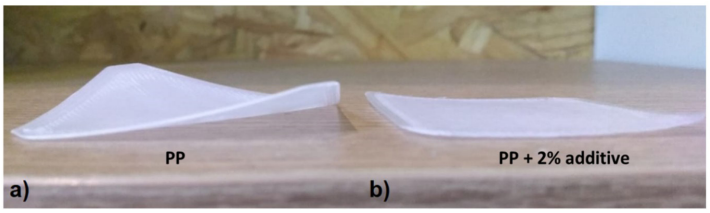

Figure 3. Comparison of 3D-printed polypropylene (PP) samples. (a) Pure PP showing severe warping due to thermal shrinkage. (b) PP with 2% ZnO-based glassy ceramic additive (Si-Na-Al matrix) exhibiting improved dimensional stability and reduced warping, enhancing printability.

The modified material exhibited enhanced interlayer adhesion and dimensional stability, reducing shrinkage without requiring fixatives or surface treatments. This effect is attributed to the inorganic additive altering the crystallization dynamics and thermal behavior of the polymer during cooling, mitigating internal stresses. These results are consistent with previous reports, which demonstrate that incorporating inorganic oxides such as ZnO into polymer matrices enhances chemical stability, semiconductivity, and mechanical strength, directly affecting microstructure formation and dimensional stability in additive manufacturing[18]. Furthermore, recent studies highlight that the addition of nanomaterials to thermoplastic polymers improves mechanical and thermal properties, in addition to favoring adhesion between layers and reducing internal stresses, increasing dimensional stability and 3D printing quality[19].

This finding addresses a well-known limitation in additive manufacturing of polyolefins, particularly polypropylene, which typically suffers from excessive thermal shrinkage, warpage and poor interlayer adhesion. By improving dimensional stability and print quality, this material enables the use of polypropylene in applications previously limited by printability challenges. Beyond its functional properties, this improvement greatly expands the versatility of polypropylene in additive manufacturing, enabling its application in more complex geometries and diverse industries such as healthcare, consumer goods, and functional components that demand precision and stability. This processing advantage complements the material's antiviral functionality, broadening its technological relevance[20].

Figure 4 presents SEM-FEG images in backscattered electron (BSE) mode, which enhances contrast based on atomic number differences, allowing clear visualization of the inorganic additive dispersion within the polypropylene (PP) matrix.

Figure 4a corresponds to pure PP, showing a homogeneous and smooth surface without detectable particles. In contrast, Figure 4b displays the sample with 2% additive, where bright regions, indicative of elements with higher atomic number, such as Zn, Al, and Si from the glassy ceramic, begin to appear sparsely distributed. With 6% additive Figure 4c, the distribution becomes more noticeable, with a higher density of bright spots evenly dispersed across the matrix. In Figure 4d, with 10% additive, a significantly higher density of bright regions is observed, confirming the successful incorporation of the ceramic particles. Some particles are partially exposed on the composite surface, which is relevant for antiviral performance. However, localized agglomerations are also detected in certain areas. These micrographs demonstrate that the additive was effectively integrated into the polymer, with reasonably good dispersion even at higher concentrations, which is critical for ensuring functional performance of the composite material. Notably, the SEM-FEG analysis was performed on the same samples subjected to antimicrobial and antiviral tests, ensuring that the morphological observations directly represent the surfaces evaluated for biological activity.

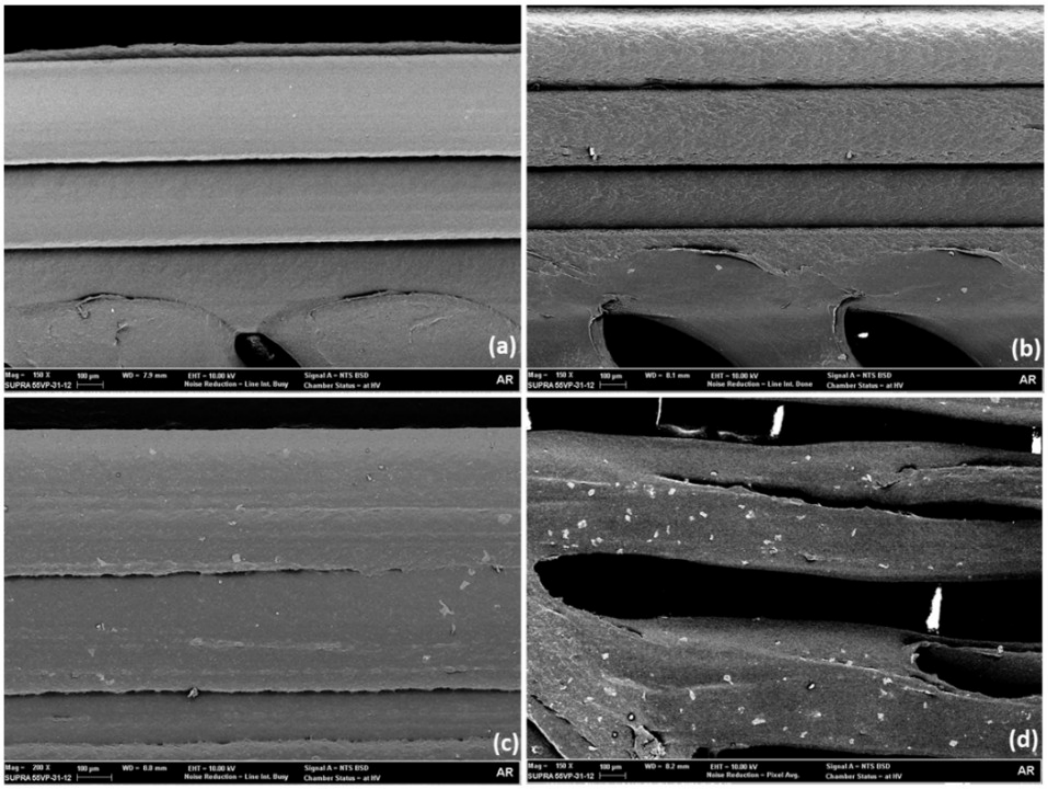

Figure 4. SEM-FEG images in backscattered electron (BSE) mode showing additive dispersion in PP. (a) Pure PP without additive; (b) PP + 2%, (c) PP + 6%, and (d) PP + 10% of ZnO-based glassy ceramic additive (Si-Na-Al matrix). Bright regions indicate the presence of the inorganic phase, with increasing particle density as additive content rises, at 150x.

Particle size measurements revealed an average maximum linear dimension (Ferret's diameter) of 20.72 ± 2.90 µm for the pure additive. In the composite samples, similar particle dimensions were observed, with averages of 21.30 ± 1.46 µm, 19.56 ± 1.96 µm, and 20.34 ± 1.76 µm for additive loadings of 2%, 6%, and 10%, respectively. Statistical analysis (ANOVA, $p = 0.063$) confirmed that these values are statistically equivalent at a 95% confidence level. This indicates that the extrusion and additive incorporation processes did not significantly alter particle size distribution, ensuring consistent morphological characteristics across all evaluated composites. Such consistency supports uniformity in the antiviral and printability performance observed for the composites at different additive concentrations.

Figure 5 presents the morphological and chemical characterization of the masterbatch composed of polyethylene (PE) and the ZnO-based glassy ceramic additive, using SEM-FEG in BSE mode combined with EDS analysis.

In Figure 5a , at 500× magnification, the bright regions correspond to the inorganic additive dispersed within the polymeric matrix. Region "1" was selected for detailed observation at higher magnification shown in Figure 5b, captured at 3000×. In this micrograph, the contrast is significantly enhanced due to the higher atomic number of the additive components (Zn, Al, Si, Na) compared to the polymer matrix. The marker "2" indicates a representative particle, and the point marked with "X" corresponds to the location where the EDS punctual analysis was performed.

The EDS spectrum in Figure 5c confirms the chemical composition of the bright particle, with prominent peaks of zinc (Zn), silicon (Si), aluminum (Al), sodium (Na), and oxygen (O), validating the composition of the additive as ZnO embedded in a glassy matrix rich in Si, Al, and Na. The presence of carbon (C) is attributed to the PE matrix, while gold (Au) and palladium (Pd) signals arise from the conductive coating applied for SEM-FEG analysis. The semi-quantitative EDS analysis of the selected particle (point X, Figure 5c) confirms the composition of the inorganic additive. The elemental composition by weight was predominantly silicon (Si, 27.8%), oxygen (O, 24.9%), carbon (C, 20.2%), sodium (Na, 8.2%), palladium (Pd, 2.8%), aluminium (Al, 1.3%), and zinc (Zn, 1.1%). The strong Zn peaks, combined with Al and Si, correlate directly with the higher contrast regions in the BSE images, evidencing the presence and proper incorporation of the ceramic additive. Additionally, the distribution and morphology observed suggest a good level of dispersion of the additive within the polymer, which is critical for ensuring the functional properties of the composite material.

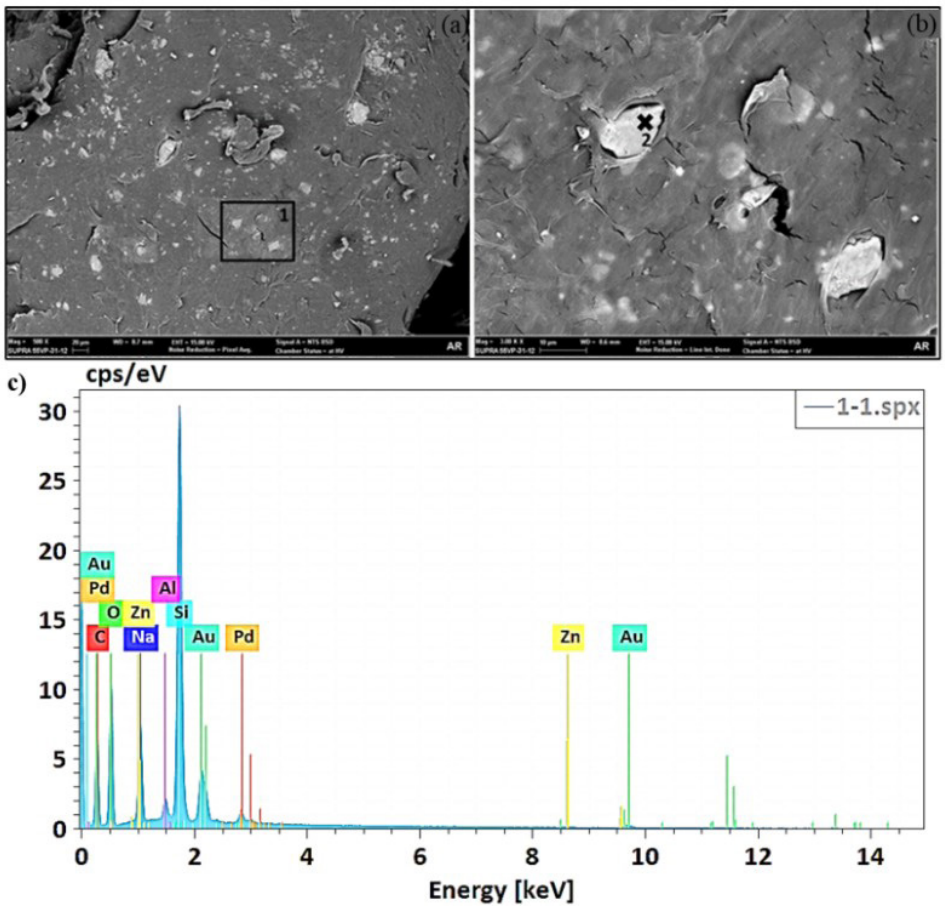

Figure 5. Figure X. SEM-FEG images in BSE mode and EDS analysis of the PE masterbatch with ZnO-based glassy ceramic additive. (a) Overview at 500× showing dispersed inorganic particles; (b) detail at 3000× with EDS point marked "X". (c) EDS spectrum confirming Zn, Si, Al, Na, and O from the additive.

The FTIR spectra in Figure 6 were analyzed for pure PP homopolymer, PP with additive loadings of 2%, 6% and 10% as well as the PE masterbatch containing additive.

The FTIR spectrum of neat PP exhibits its characteristic absorption bands at 2950, 2915, and 2838 cm^{-1}, corresponding to asymmetric and symmetric C–H stretching vibrations of methyl (CH_3) and methylene (CH_2) groups. Bending vibrations are observed at 1455 cm^{-1} (CH_2) and 1377 cm^{-1} (CH_3), which is a diagnostic band for the isotactic polypropylene structure. Additional bands at 1167, 997, 972, 840, and 808 cm^{-1} are associated with CH_3 rocking modes and C–C stretching vibrations within the polymer backbone[21].

The additive's spectrum is dominated by typical PE features at 2915 and 2848 cm^{-1} (C–H stretching), 1472 and 1462 cm^{-1} (CH_2 bending), and 730/719 cm^{-1} (CH_2 rocking). Superimposed on these are distinct bands related to the inorganic components. Specifically, broad absorption bands between 1000 and 1200 cm^{-1} are attributed to Si–O–Si asymmetric stretching, indicative of the silicate network from the glass matrix[22].

As the concentration of the additive increases (2%, 6%, and 10% by weight), a progressive enhancement is observed not only in the intensity of the inorganic bands, particularly the Si–O–Si (1000–1200 cm^{-1}), but also in the C–H stretching region between 2800 and 3000 cm^{-1}. This increase in the 2915 and 2848 cm^{-1} bands is directly correlated with the polyethylene content introduced by the additive, reflecting the cumulative contribution of the PE carrier to the composite's overall chemical signature. Importantly, despite this amplification, the main vibrational features of the polypropylene matrix remain unchanged, indicating that the additive is physically dispersed without inducing chemical modifications to the PP macromolecular structure. The appearance and systematic growth of the silicate (Si–O–Si), zinc oxide (Zn–O), and C–H stretching bands serve as robust spectral markers for the additive's incorporation and homogeneous distribution within the composite material.

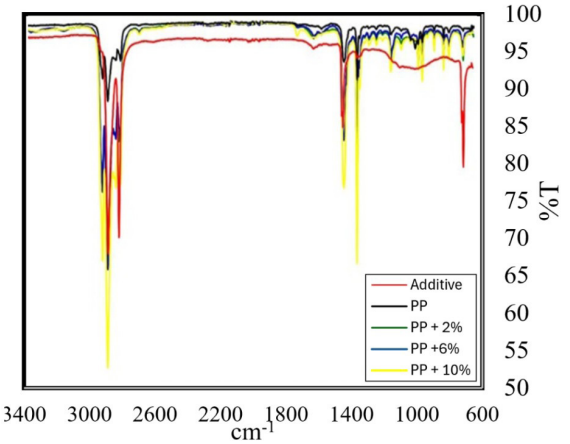

Figure 6. FTIR spectra of PP, the ZnO-based glassy ceramic additive, PP composites with 2%, 6%, and 10% additive and PE masterbatch containing additive.

Table 2 presents the results obtained for *Escherichia coli* and *Staphylococcus aureus*, including initial and final bacterial counts with and without treatment. The antimicrobial evaluation of polymers containing 2%, 6%, and 10% of the active agent showed no effectiveness in reducing bacterial counts. After exposure to the polymer surfaces, bacterial populations remained comparable to the control groups, indicating that the tested concentrations were insufficient to inhibit microbial growth.

The results indicate that none of the tested polymer films exhibited antimicrobial activity against the evaluated bacteria. This effect may be attributed to the encapsulation of ZnO within the polymer matrix, forming a physical barrier that restricts its interaction with bacterial cells and hinders the efficient release of reactive oxygen species, which are essential for its antimicrobial action. Previous studies highlighted that controlled ZnO release is crucial for optimizing its bactericidal activity[23,24]. As mentioned, ZnO encapsulated in a glassy matrix did not exhibit classical antimicrobial activity, particularly against bacteria, likely due to its heterogeneous dispersion and limited ion release in aqueous media, factors that typically influence bactericidal efficacy[25]. Moreover, combining ZnO with other antimicrobial compounds may offer a promising solution. Studies indicate that hybrid materials, such as ZnO combined with silver nanoparticles, exhibit a synergistic effect, enhancing antimicrobial action against E. coli and S. aureus. Developing combined formulations is a valuable strategy to optimize the functionality of antimicrobial polymers[26]. The observed results highlight the need for further investigations into the impact of the polymer matrix on ZnO functionality in bacterial inhibition. To overcome these limitations, future strategies could focus on enhancing the surface exposure of the inorganic phase through post-printing surface treatments or developing hybrid formulations that incorporate antimicrobial agents with mechanisms independent of ion release, such as photocatalytic materials. These approaches could significantly improve antibacterial performance without compromising the structural integrity or printability of the polypropylene composite[27].

The results presented in Table 3 demonstrate the antiviral efficacy of polypropylene (PP) samples with 2%, 6% and 10% additive concentrations against both MHV-3 (enveloped) and adenovirus (non-enveloped) after 15 and 120 minutes of exposure.

Table 2. Antimicrobial activity of E. coli and S. aureus at time 0 and after 24 hours of exposure, expressed as CFU count.

Sample	Exposure time (hours)	E.Coli (CFU Count)	S.aureus (CFU Count)
PP	0	$1.72\ 10^6$	$5.31\ 10^7$
	24	$8.44\ 10^7$	$1.41\ 10^9$
PP + 2%	24	$1.31\ 10^9$	$1.23\ 10^9$
PP + 6%	24	$7.20\ 10^8$	$1.47\ 10^9$
PP + 10%	24	$8.63\ 10^8$	$1.63\ 10^9$

The PP + 10% sample showed the highest reduction in viral load, with 2.5 log for MHV-3 and 1.5 log for adenovirus after 120 minutes. This equates to a viral reduction of 99.68% for MHV-3 and 96.84% for adenovirus, confirming the enhanced antiviral properties of the treated materials, particularly with longer exposure times. Despite the lack of antibacterial activity observed against E. coli and S. aureus (Table 2), the material exhibited significant antiviral efficacy, particularly against betacoronaviruses. This difference can be attributed to the distinct mechanisms by which zinc oxide (ZnO) interacts with bacterial versus viral structures. In bacterial systems, the antimicrobial action of ZnO primarily depends on the release of Zn^{2+} ions, penetration of the cell wall, and metabolic disruption[28].

Qualitative visual confirmation of the antiviral activity is provided by microscopy images on Figure 7, clearly demonstrating that untreated PP exhibited a significant cytopathic effect caused by betacoronavirus, whereas the PP composite with 10% additive displayed a notably reduced cytopathic effect. This aligns with the quantitative antiviral results (Table 3), reinforcing the effectiveness of the ceramic additive.

However, when ZnO is embedded in a polymeric matrix, its release is significantly hindered, limiting its interaction with bacterial membranes, especially those with robust structural barriers and antioxidant defenses. In contrast, antiviral mechanisms do not rely solely on ion release. Enveloped viruses, like betacoronaviruses and adenovirus, are particularly susceptible to surface interactions that disrupt lipid and protein components of the viral envelope. The surface of the glassy ceramic additive, composed of ZnO within a Si-Na-Al matrix, may facilitate electrostatic interactions and localized oxidative stress, leading to viral inactivation even with limited Zn^{2+} release. Additionally, ZnO can generate reactive oxygen species (ROS) under certain conditions, such as light exposure or moderate heat, which can damage viral envelope proteins and RNA, contributing to its antiviral effect[29]. This antiviral performance is likely enhanced by the presence of exposed inorganic particles on the surface, as evidenced in the SEM-BSE images (Figure 3), which facilitate direct contact with viral particles[30]. This contact-driven mechanism, combined with localized oxidative stress, may be particularly effective against enveloped viruses. Furthermore, the glassy matrix itself may play a synergistic role by modulating the surface environment, enhancing viral adsorption and promoting structural destabilization through physicochemical mechanisms like surface charge variations or local pH shifts. This synergy may explain why significant antiviral activity was observed, while the antibacterial response remained limited. Recent literature supports that the effectiveness of metal oxides, including ZnO, varies substantially depending on the type of microorganism and the material's form of presentation[31].

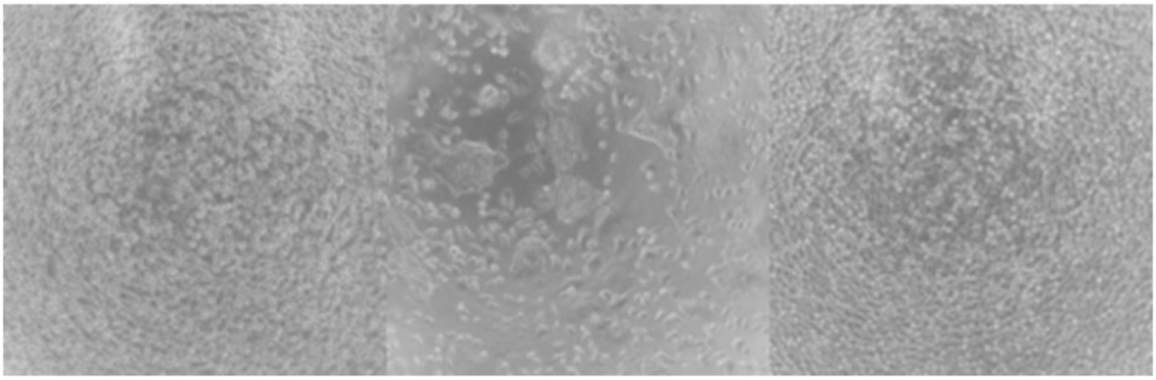

Figure 7. Representative microscopy images demonstrating antiviral efficacy against betacoronavirus (MHV-3). (a) Cell control without virus exposure; (b) PP without additive showing clear cytopathic effect due to viral replication; (c) PP with 10% ZnO-based glassy ceramic additive (Si–Na–Al matrix), showing significantly reduced cytopathic effect after 120 min of virus contact.

Table 3. Viral titration results of adenovirus and MHV-3 after evaluated exposure times, presenting R values and the percentage reduction in viral load for each treated sample compared to the control sample.

Sample	Exposure time (Minutes)	MHV-3		Adenovirus	
		R	%	R	%
PP + 2%	15	1.00	90.00	0.50	68.42
	120	1.00	90.00	1.00	90.00
PP + 6%	15	1.00	90.00	1.50	96.84
	120	1.50	96.84	1.50	96.84
PP + 10%	15	2.00	99.00	1.50	96.84
	120	2.50	99.68	1.50	96.84

4. Conclusions

This study demonstrated the development of polypropylene (PP) filaments functionalized with a ZnO-based glassy ceramic additive (Si–Na–Al matrix) tailored for extrusion-based additive manufacturing. The incorporation of the additive significantly reduced thermal shrinkage and improved interlayer adhesion, addressing a long-standing limitation in 3D printing of polyolefins. In addition, the composites exhibited remarkable antiviral activity, with viral reductions of up to 99.68% against betacoronavirus and 96.84% against adenovirus at the highest additive concentration. These results highlight the potential of ceramic-modified PP filaments to combine structural integrity with antiviral functionality.

In contrast, no significant antibacterial activity was observed against E. coli and S. aureus, likely due to limited release of Zn^{2+} ions from the polymeric matrix. While this restricts the antibacterial response, the specific antiviral performance remains highly relevant, particularly in applications where viral contamination poses a greater risk than bacterial proliferation. Future research should explore strategies to enhance antibacterial efficacy, such as surface modification or hybrid formulations incorporating additional antimicrobial agents, while preserving the improved printability achieved in this study.

Overall, this work provides a viable pathway for producing functional PP-based composites that integrate manufacturability with antiviral properties. Such materials hold promise for applications in healthcare, packaging, and consumer products, contributing to the development of next-generation functional polymers for additive manufacturing.

5. Acknowledgments

The authors would like to thank the equipment provided by Nucleo Vitro, Senai Institute of Innovation, UniSENAI and IFSC.

6. References

1. Najmon JC, Raeisi S, Tovar A. Review of additive manufacturing technologies and applications in the aerospace industry. In: Froes M, Boyer R, eds. Additive Manufacturing for the Aerospace Industry [Internet]. Amsterdam: Elsevier; 2019 [cited 2024 Aug 16]. p. 7-31. Available from: https://linkinghub.elsevier.com/retrieve/pii/B9780128140628000029.
2. Chong WJ, Shen S, Li Y, Trinchi A, Pejak D, (Louis) Kyratzis I, et al. Additive manufacturing of antibacterial PLA-ZnO nanocomposites: Benefits, limitations and open challenges. J Mater Sci Technol. 2022;111:120-51. https://doi.org/10.1016/j.jmst.2021.09.039.
3. González-Henríquez CM, Sarabia-Vallejos MA, Rodríguez Hernandez J. Antimicrobial polymers for additive manufacturing. Int J Mol Sci. 2019;20(5):1210. https://doi.org/10.3390/ijms20051210.
4. Guidotti G, Soccio M, Lotti N, Gazzano M, Siracusa V, Munari A. Poly(propylene 2,5-thiophenedicarboxylate) vs. Poly(propylene 2,5-furandicarboxylate): two examples of high gas barrier bio-based polyesters. Polymers (Basel). 2018;10(7):785. https://doi.org/10.3390/polym10070785.
5. Siracusa V, Blanco I. Bio-Polyethylene (Bio-PE), Bio-Polypropylene (Bio-PP) and Bio-Poly(ethylene terephthalate) (Bio-PET): Recent Developments in Bio-Based Polymers Analogous to Petroleum-Derived Ones for Packaging and Engineering Applications. Polymers (Basel). 2020;12(8):1641. https://doi.org/10.3390/polym12081641.
6. McFarland AW Jr, Elumalai A, Miller CC, Humayun A, Mills DK. Effectiveness and applications of a metal-coated HNT/Polylactic acid antimicrobial filtration system. Polymers (Basel). 2022;14(8):1603. https://doi.org/10.3390/polym14081603.
7. Vidakis N, Petousis M, Velidakis E, Mountakis N, Tzounis L, Liebscher M, et al. Enhanced mechanical, thermal and antimicrobial properties of additively manufactured polylactic acid with optimized nano silica content. Nanomaterials (Basel). 2021;11(4):1012. https://doi.org/10.3390/nano11041012.
8. Youssef Ahmed M, EL-Sayed SM, EL-Sayed HS, Salama HH, Dufresne A. Enhancement of Egyptian soft white cheese shelf life using a novel chitosan/carboxymethyl cellulose/zinc oxide bionanocomposite film. Carbohydr Polym. 2016;151:9-19. https://doi.org/10.1016/j.carbpol.2016.05.023.
9. Youssef AM, Malhat FM, Abdel Hakim AA, Dekany I. Synthesis and utilization of poly (methylmethacrylate) nanocomposites based on modified montmorillonite. Arab J Chem. 2017;10(5):631-42. https://doi.org/10.1016/j.arabjc.2015.02.017.
10. Roy S, Shankar S, Rhim JW. Melanin-mediated synthesis of silver nanoparticle and its use for the preparation of carrageenan-based antibacterial films. Food Hydrocoll. 2019;88:237-46. https://doi.org/10.1016/j.foodhyd.2018.10.013.
11. Sofi SA, Singh J, Rafiq S, Ashraf U, Dar BN, Nayik GA. A comprehensive review on antimicrobial packaging and its use in food packaging. Curr Nutr Food Sci. 2018;14(4):305-12. https://doi.org/10.2174/1573401313666170609095732.
12. Jideani VA, Vogt K. Antimicrobial packaging for extending the shelf life of bread: a review. Crit Rev Food Sci Nutr. 2016;56(8):1313-24. https://doi.org/10.1080/10408398.2013.768198.
13. Chen XG, Zheng L, Wang Z, Lee CY, Park HJ. Molecular affinity and permeability of different molecular weight chitosan membranes. J Agric Food Chem. 2002;50(21):5915-8. https://doi.org/10.1021/jf020151g.
14. Torres MA, Vieira RS, Beppu MM, Santana CC. Produção e caracterização de microesferas de quitosana modificadas quimicamente. Polímeros. 2005;15(4):306-12. https://doi.org/10.1590/S0104-14282005000400016.
15. Zouine N, Er Raouan S, El Ghachtouli N, El Abed S, Ibn Souda Koraichi S. Enhancing 3D printed PET physicochemical properties to prevent bacterial adhesion: phenolic compound-based approach. Int J Adhes Adhes. 2025;136:103847. https://doi.org/10.1016/j.ijadhadh.2024.103847.
16. ISO: International Organization for Standardization. ISO 22196: 2011(E): Measurement of antibacterial activity on plastics and other non-porous surfaces. Switzerland: ISO; 2011.
17. ISO: International Organization for Standardization. ISO 21702:2019: Measurement of antiviral activity on plastics and other non-porous surfaces. Switzerland: ISO; 2019.
18. Vidakis N, Petousis M, Maniadi A, Koudoumas E, Kenanakis G, Romanitan C, et al. The mechanical and physical properties of 3D-printed materials composed of ABS-ZnO nanocomposites and ABS-ZnO microcomposites. Micromachines (Basel). 2020;11(6):615. https://doi.org/10.3390/mi11060615.
19. Luo X, Cheng H, Wu X. Nanomaterials reinforced polymer filament for fused deposition modeling: a state-of-the-art review. Polymers (Basel). 2023;15(14):2980. https://doi.org/10.3390/polym15142980.
20. Fernando S, Gunasekara T, Holton J. Antimicrobial Nanoparticles: applications and mechanisms of action. Sri Lankan J Infect Dis. 2018;8(1):2. https://doi.org/10.4038/sljid.v8i1.8167.
21. Lin JH, Pan YJ, Liu CF, Huang CL, Hsieh CT, Chen CK, et al. Preparation and compatibility evaluation of polypropylene/high density polyethylene polyblends. Materials (Basel). 2015;8(12):8850-9. https://doi.org/10.3390/ma8125496.
22. Hecker C, Der Meijde MV, Van Der Meer FD. Thermal infrared spectroscopy on feldspars: Successes, limitations and their implications for remote sensing. Earth Sci Rev. 2010;103(1–2):60-70. https://doi.org/10.1016/j.earscirev.2010.07.005.

23. Jones N, Ray B, Ranjit KT, Manna AC. Antibacterial activity of ZnO nanoparticle suspensions on a broad spectrum of microorganisms. FEMS Microbiol Lett. 2008;279(1):71-6. https://doi.org/10.1111/j.1574-6968.2007.01012.x.
24. Raghupathi KR, Koodali RT, Manna AC. Size-dependent bacterial growth inhibition and mechanism of antibacterial activity of zinc oxide nanoparticles. Langmuir. 2011;27(7): 4020-8. https://doi.org/10.1021/la104825u.
25. Faure B, Salazar-Alvarez G, Ahniyaz A, Villaluenga I, Berriozabal G, De Miguel YR, et al. Dispersion and surface functionalization of oxide nanoparticles for transparent photocatalytic and UV-protecting coatings and sunscreens. Sci Technol Adv Mater. 2013;14(2):023001. https://doi.org/10.1088/1468-6996/14/2/023001.
26. Sirelkhatim A, Mahmud S, Seeni A, Kaus NHM, Ann LC, Bakhori SKM, et al. Review on zinc oxide nanoparticles: antibacterial activity and toxicity mechanism. Nano-Micro Lett. 2015;7(3):219-42. https://doi.org/10.1007/s40820-015-0040-x.
27. Caracciolo PC, Abraham GA, Battaglia ES, Bongiovanni Abel S. Recent progress and trends in the development of electrospun and 3D printed polymeric-based materials to overcome Antimicrobial Resistance (AMR). Pharmaceutics. 2023;15(7):1964. https://doi.org/10.3390/pharmaceutics15071964.
28. Amrhar R, Singh J, Eesaee M, Carrière P, Saidi A, Nguyen-Tri P. Polymeric nanocomposites-based advanced coatings for antimicrobial and antiviral applications: a comprehensive overview. Results in Surfaces and Interfaces. 2025;19:100497. https://doi.org/10.1016/j.rsurfi.2025.100497.
29. Vibornijs V, Zubkins M, Strods E, Rudevica Z, Korotkaja K, Ogurcovs A, et al. Analysis of antibacterial and antiviral properties of ZnO and Cu coatings deposited by magnetron sputtering: evaluation of cell viability and ROS production. Coatings. 2023;14(1):14. https://doi.org/10.3390/coatings14010014.
30. Ghaffari H, Tavakoli A, Moradi A, Tabarraei A, Bokharaei-Salim F, Zahmatkeshan M, et al. Inhibition of H1N1 influenza virus infection by zinc oxide nanoparticles: another emerging application of nanomedicine. J Biomed Sci. 2019;26(1):70. https://doi.org/10.1186/s12929-019-0563-4.
31. Ramani M, Ponnusamy S, Muthamizhchelvan C, Marsili E. Amino acid-mediated synthesis of zinc oxide nanostructures and evaluation of their facet-dependent antimicrobial activity. Colloids Surf B Biointerfaces. 2014;117:233-9. https://doi.org/10.1016/j.colsurfb.2014.02.017.

Data Availability

The datasets supporting the findings of this study are available from the corresponding author upon reasonable request. The data are not publicly available due to confidentiality obligations associated with public–private partnerships and contractual restrictions related to industrial service agreements.